Overview of the FTU results – 2022

- ✓ Liquid metal limiters
- ✓ Runaway electrons studies
  Measurements of plasma waves emitted by runaways
- ✓ Tearing modes stabilization by ECH
  Tearing modes stabilization by pellet injection
  MHD limit cycles
- ✓ Behavior of heavy metal ions
  Helium doped plasmas
- ✓ EC assisted start-up in presence of Ne
  High temperature plasmas
- ✓ Diagnostics
  - Laser induced breakdown spectroscopy
  - Runaway electron imaging spectroscopy system
  - High resolution saddle coil array
  - Diamond detectors for fast VUV and SXR diagnostics

Liquid metal limiters

- Liquid metal investigation as plasma-facing materials on FTU: the first tokamak performing experiments using a liquid lithium limiter and a liquid tin limiter.
- Plasma performances unaffected (without core accumulation) for liquid tin surface temperatures below the evaporation onset, with heat loads up to 18 MW/m^2 for 1 s.
- Liquid Metal divertor concept design, CPS-based (WP-DTT1-LMD).

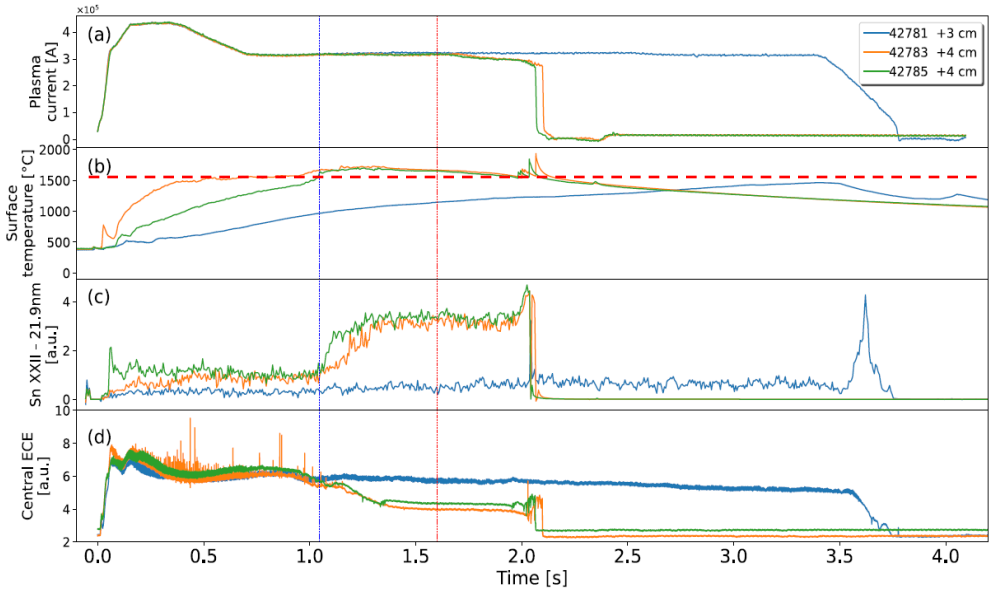

Mazzitelli G. NF **59** (2019)
Roccella S. JFE **39** (2020)

Figure 1. *Experiments performed by moving, pulse by pulse, the limiter towards the plasma column to increase the heat load on the liquid tin surface. The strong increase in the plasma impurity content is observed when the surface temperature exceeds the tolerable operative range, with a subsequent loss of the sawtooth activity and plasma disruption.*

Runaway electrons studies

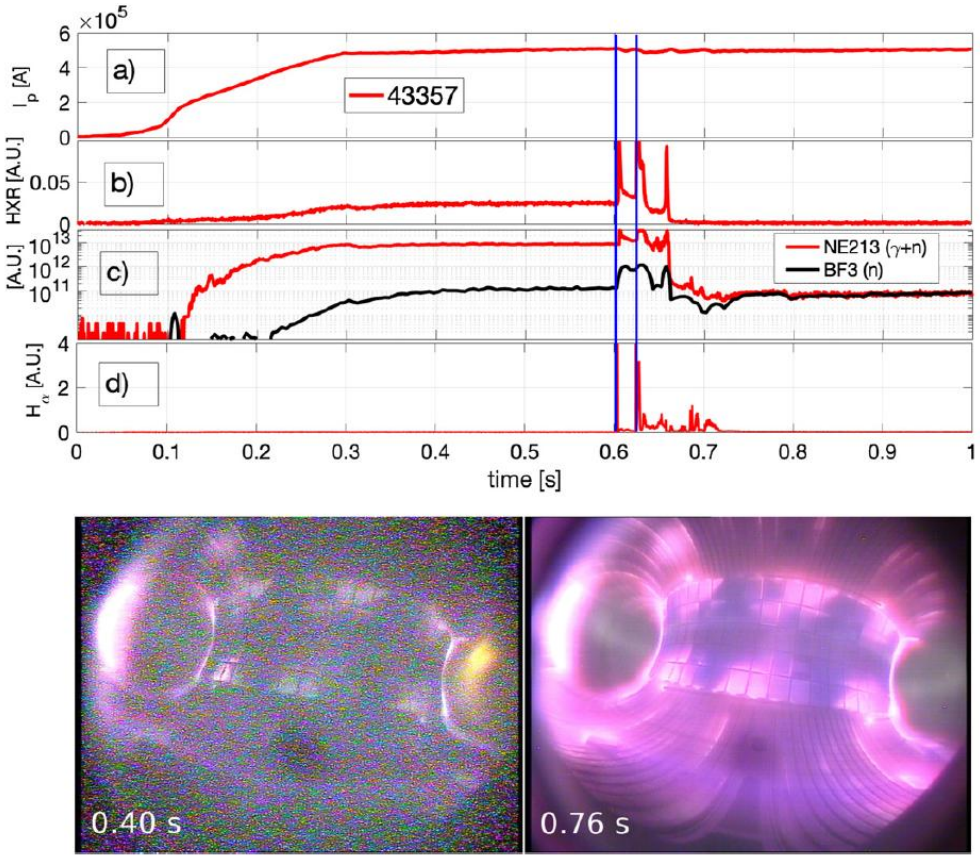

- D_2 pellets injected on flat-top current pulses with different RE population, by varying pellet size, number and inter-times, to study the capability of REs dissipation/mitigation and the ablation rate of pellets, useful for ITER.

- Complete RE loss induced by multiple pellet injection.

Carnevale D. NF **61** (2021)

Figure 2. *D_2 pellet injections at times 0.60 s and 0.62 s on RE quiescent discharge: almost unperturbed plasma current, complete loss of REs as shown by collapse of signal NE213 on signal BF3 and corresponding decrease to zero of HXR signal, H_α signal.*

Plasma waves emitted by runaways

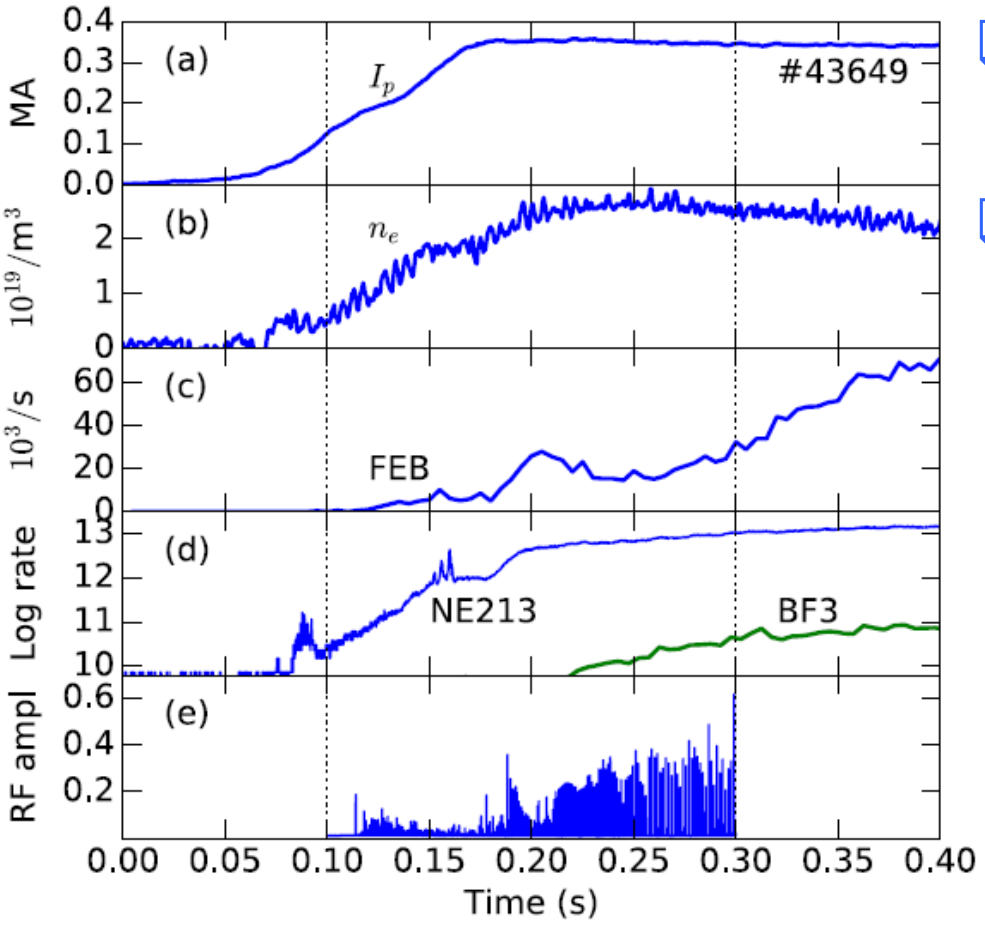

Figure 3. *Measurements of plasma waves emitted by runaway electrons. FTU pulse 43649 at 5.3 T. Vertical dotted lines mark the acquisition interval.*

- Emission of radio waves (0.4-3.0 GHz) in pulses with significant RE signatures.
- Multi-machine comparison are required to assess the relative importance of involved wave branches (whistler, magnetized plasma waves).

Buratti P. PPCF **63** (2021)

TM stabilization by ECH

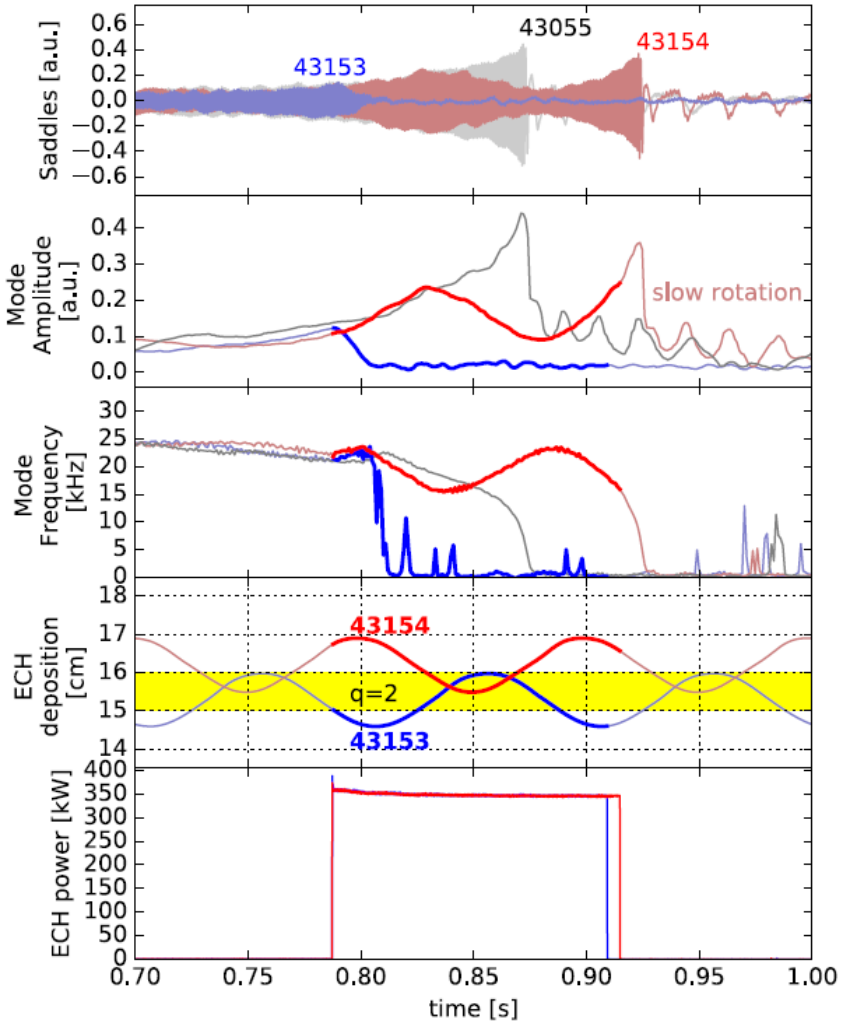

- Tearing modes stabilization by ECH in sawtooth free scenarios at low density, with a "sweeping" strategy, allowing to relax the accuracy on the estimates of the island O-point position.
- The technique was also applied on quasi locked modes, showing a partial reduction of the mode amplitude.

Alessi E., Pucella G.

Figure 4. *Tearing modes stabilization by electron cyclotron heating. Pulse 43055 (gray) is taken as reference (no ECH injected); in 43154 (red) ECH is injected in the outer proximity of the magnetic island; in pulse 43153 (blue) ECH antenna aims at the island O-point when gyrotron power is switched on.*

TM stabilization by pellet injection

- Complete/partial TM stabilization after a pellet injection in presence of a fastly/slowly rotating magnetic island. Tearing stability analysis are necessary to get some insight in the in the stabilization process

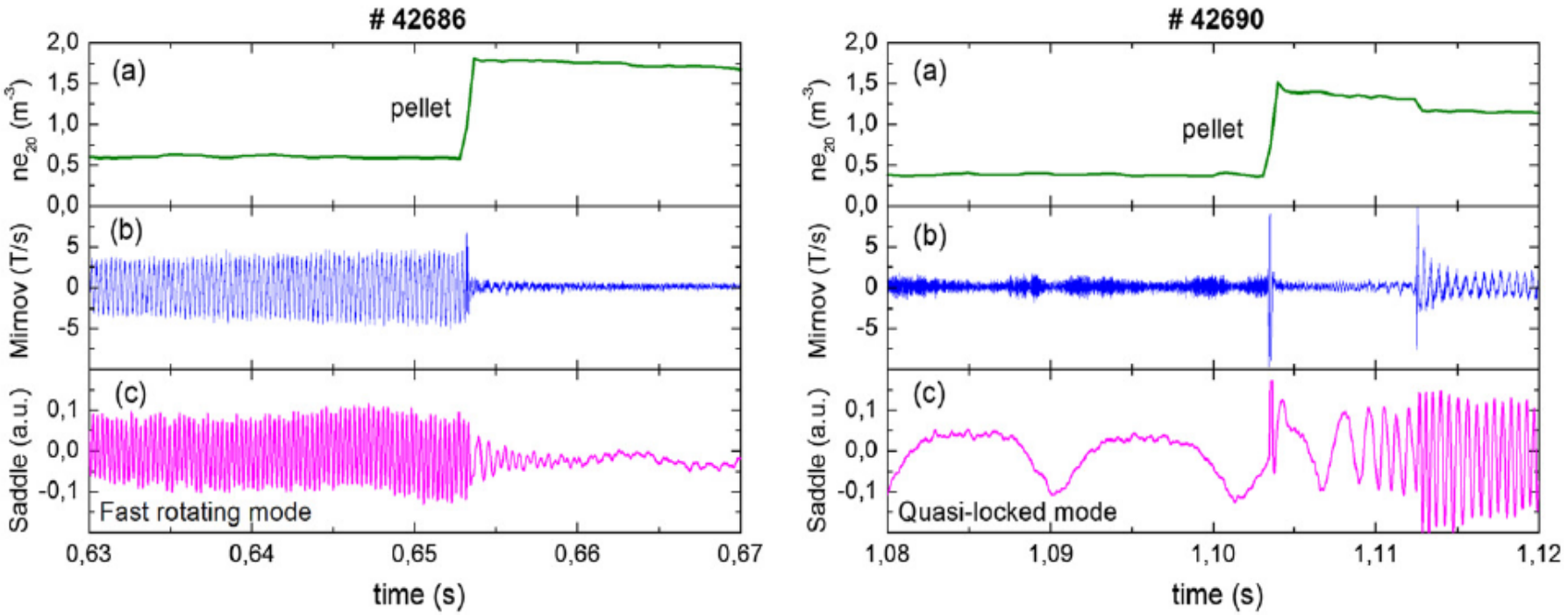

Figure 5. *Tearing modes stabilization by pellet injection. FTU pulses with a fastly rotating mode (left) and with a quasi-locked mode (right), respectively. The pellet injection corresponds to the rapid increase in density.*

Pucella G., Buratti P., Boncagni L.

MHD limit cycles

- New observations on “MHD limit cycles” starting with sawtooth-free low-density pulses. A transition from smooth to limit-cycle behavior for a 2/1 TM has been observed after Ne injection, in correspondence with the appearance of ST activity.

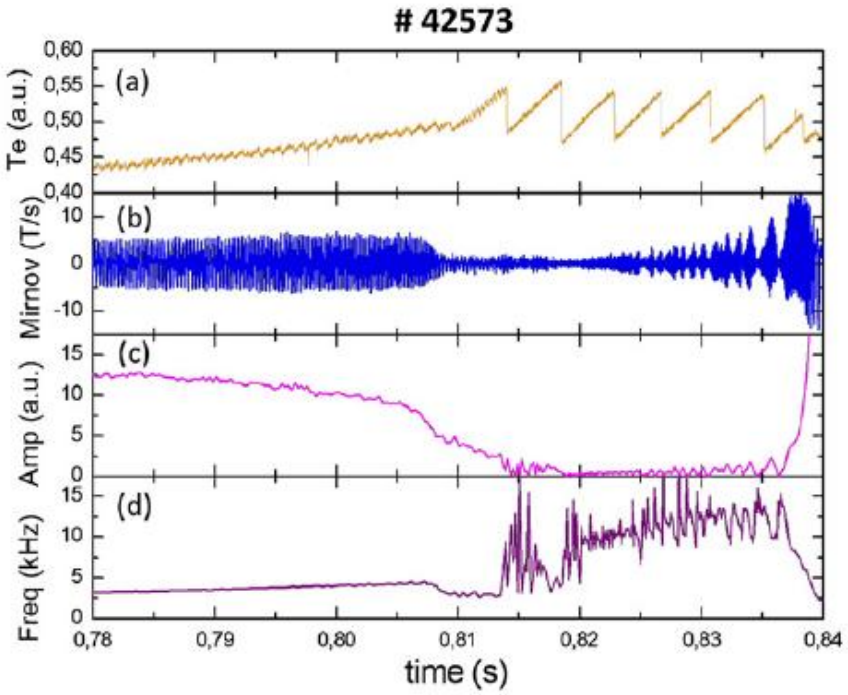

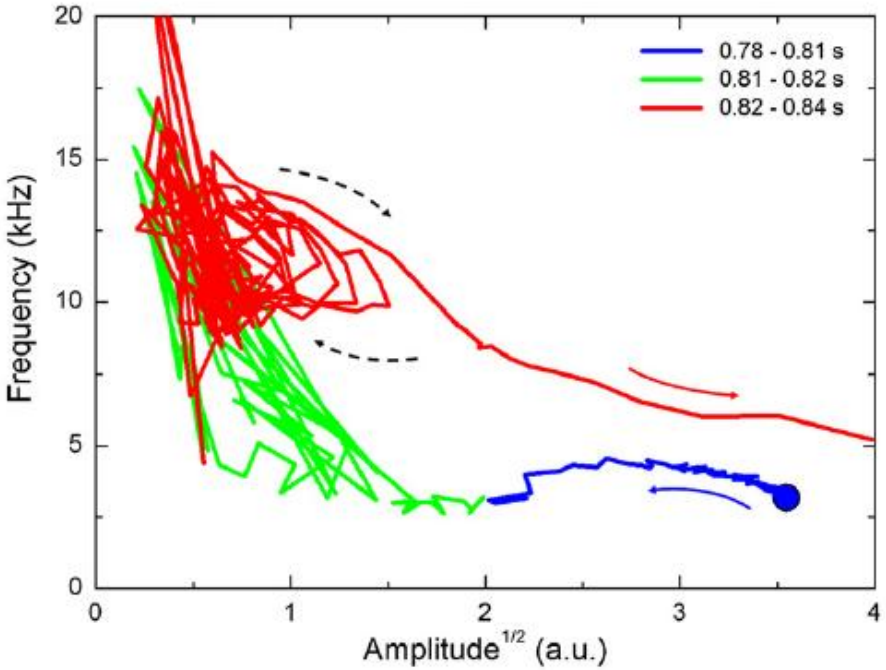

Figure 6. *MHD limit cycles. FTU pulse 42573 (B_T = 6 T, I_p = 0.50 MA). Neon injected from 0.72 to 0.75 s.*

Pucella G., Buratti P., Boncagni L.

Spectroscopy of heavy metal ions

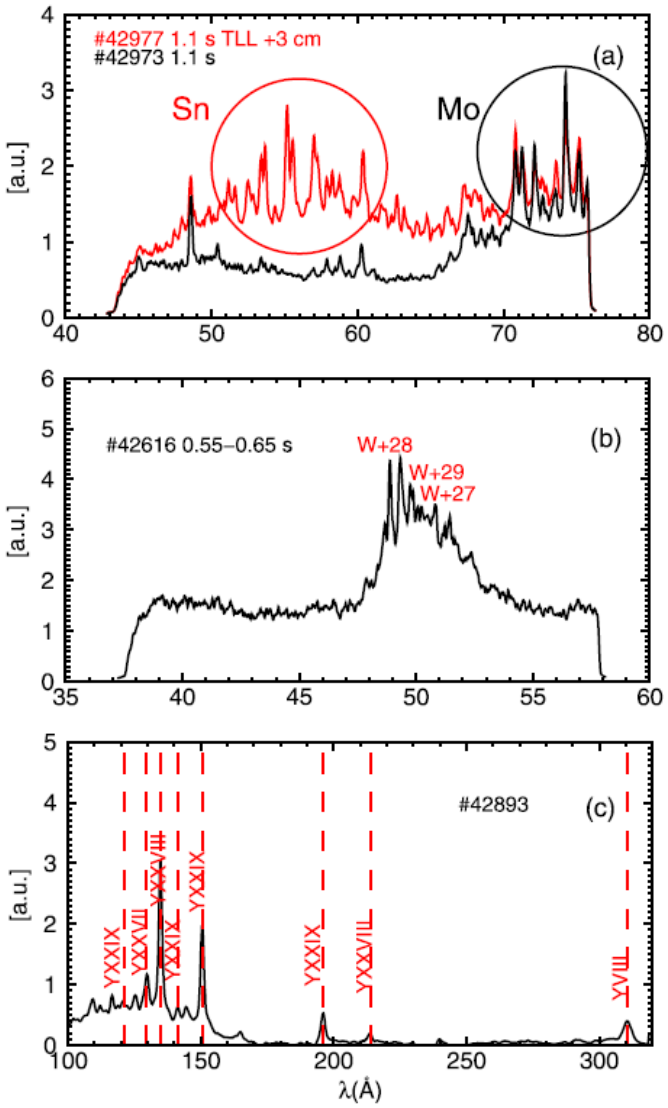

- Lines of Sn (from tin limiter) measured by SOXMOS spectrometer, identified as emission from ionization states localized between r/a = 0.75 and 0.85.
- Ion stages for W (injected by LBO technique) localized at the core/medium radius regions (coronal equilibrium calculations).
- Few lines of Y (injected by LBO) clearly visible with SPREAD spectrometer at higher wavelengths; no distinct lines at lower wavelengths.

Carraro L. IAEA CN-123/45 (2021)

Figure 7. *High resolution spectroscopy of heavy metal ions. Spectra of Sn and W taken with the SOXMOS spectrometer and spectrum of Y taken with the SPRED spectrometer.*

Helium doped plasmas

- Properties of He doped plasmas studied by varying both the amount of injected He and the rate of injections. Good assessment in the estimation of the species concentrations linking effective charge, radiation losses and VUV spectroscopy.

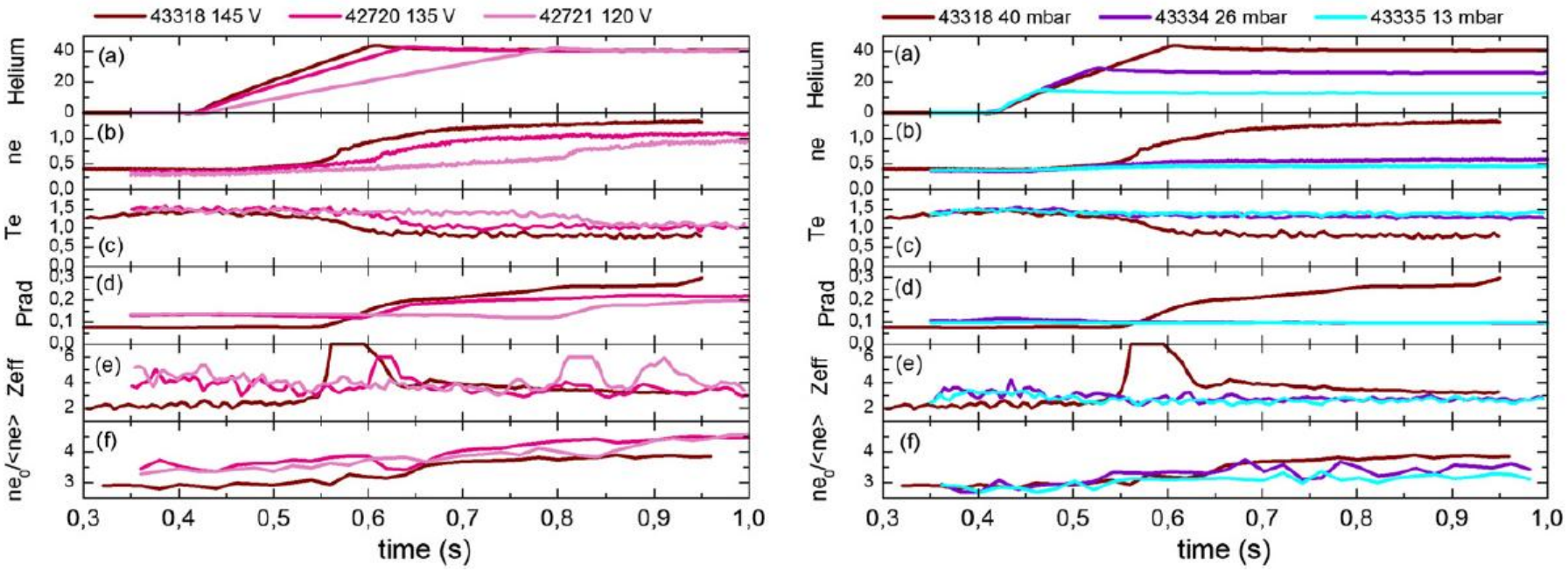

Figure 8. *(Left) Valve voltage scan for a fixed amount of total helium injected. (Right) Helium scan for a fixed valve voltage.*

Mazzotta C. NF **62** (2022)

EC assisted start-up in presence of Ne

- Experiments on EC assisted start-up performed at reduced electric field in presence of Ne impurity, to mimic the post disruption condition in superconducting future tokamaks.
- The effectiveness of EC does not strongly depend on polarization. A reduction of the internal inductance is observed by moving the EC resonance off-axis.

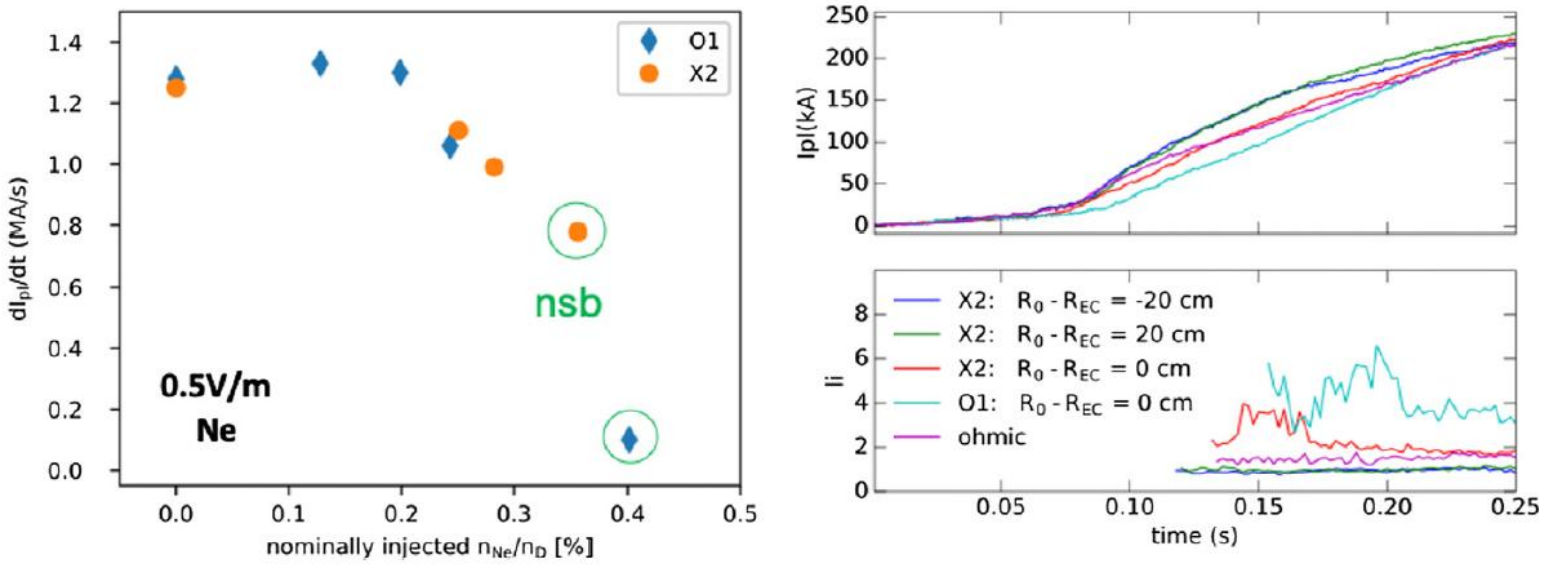

Figure 9. *(Left) Current rise as a function of impurity content in EC assisted experiment. Points in green circles represent the conditions where the start-up is not sustained. (Right) Time traces of plasma current and internal inductance for off-axis and on-axis EC resonances.*

Ricci D. EPS O5.103 (2019)

High temperature plasmas

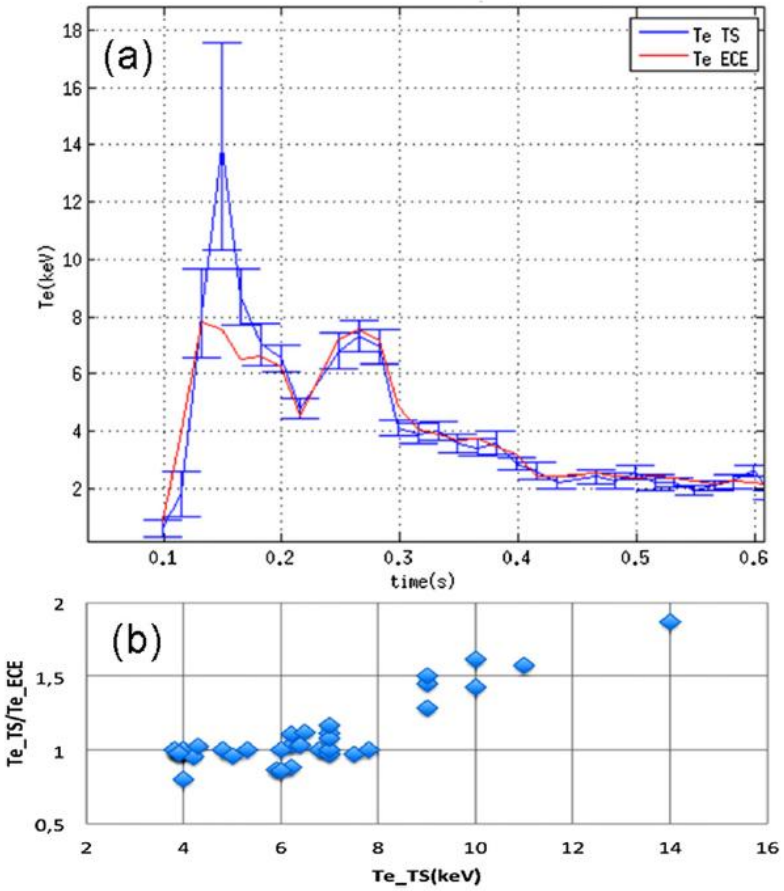

Figure 10. *(a) Electron temperature versus time for FTU pulse 43100: Te from TS in blue, Te from ECE in red. (b) Ratio Te_{TS}/Te_{ECE} versus Te_{TS} for FTU pulses 43099, 43100, 43101.*

- Systematic disagreement between the Thomson Scattering and Electron Cyclotron Emission temperature measurements at high temperature (Te_{TS} > 8 keV) in EC heated pulses on current ramp-up.
- An explanation in terms of a distortion of the electron distribution function could be considered.

Orsitto F.P., Granucci G.

LIBS and REIS

- The effectiveness of the Laser Induced Breakdown Spectroscopy system mounted on the FTU robotic arm has been demonstrated. The analysis of the FTU PFCs revealed their main chemical components, including Mo and Li.

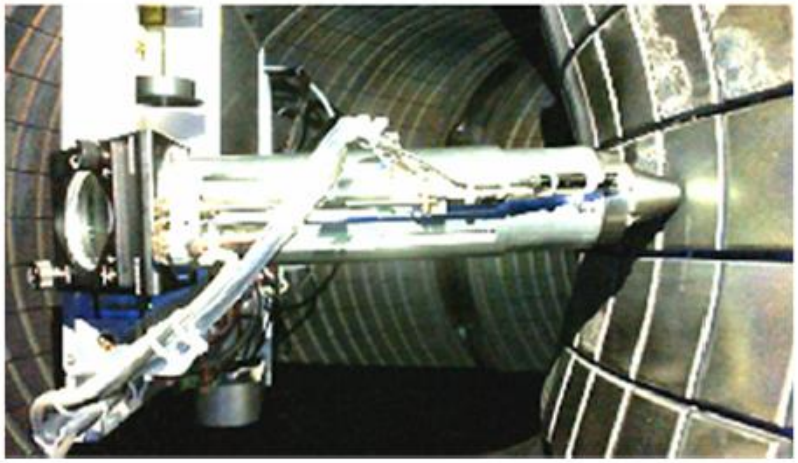

Figure 11. *The LIBS device measuring inside the FTU vacuum vessel on a tile of the toroidal limiter.*

Almaviva S. FED **57** (2020)

- The new capabilities of the Runaway Electron Imaging Spectroscopy system for in-flight RE studies have been explored, performing reconstructions of RE energy evolution based on camera and spectrometers data.

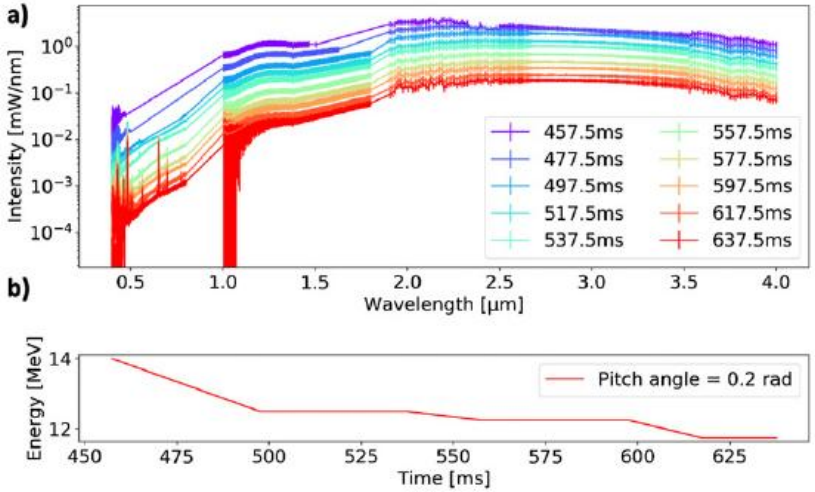

Figure 12. *RE signal interpolated from the three forward view spectrometers and RE energy reconstruction.*

Ghillardi G. PPCF **67** (2025)

Saddle coils and diamond detectors

- A high-resolution saddle coil array for MHD analysis has been utilized, showing the capability to evaluate the toroidal and poloidal mode number of TM in a large range of frequencies.

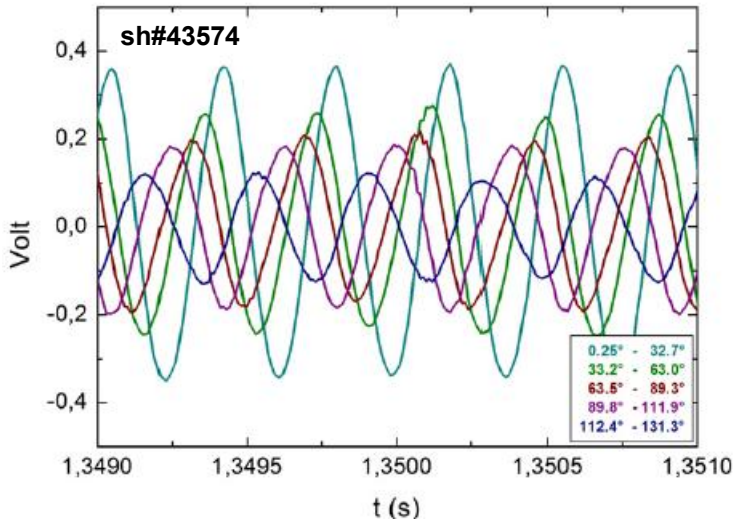

Figure 13. Signals from saddle coils at different poloidal locations in presence of a 2/1 tearing mode.

Pucella G., Giovannozzi E., Boncagni L.

- UV and SXR diamond detectors have been successfully installed and tested on different plasma scenarios, opening the possibility of a much wider range of application for this type of detectors.

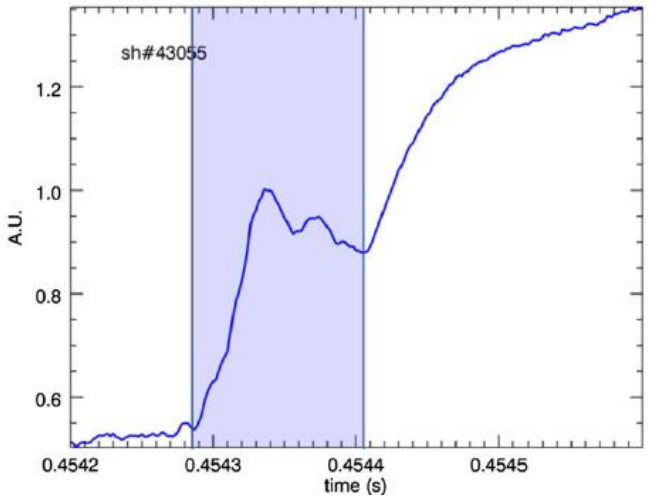

Figure 14. Ablation process of a pellet injected into an FTU plasma as recorded by the diamond detector.

Cesaroni S. FED **166** (2021)
Bombarda F. NF **61** (2021)


The End